

CHARACTERIZATION OF HIGH PROPER MOTION OBJECTS FROM THE *WIDE-FIELD INFRARED SURVEY EXPLORER*¹K. L. LUHMAN^{2,3} AND SCOTT S. SHEPPARD⁴*Draft version April 28, 2014*

ABSTRACT

We present an analysis of high proper motion objects that we have found in a recent study and in this work with multi-epoch astrometry from the *Wide-field Infrared Survey Explorer (WISE)*. Using photometry and proper motions from 2MASS and *WISE*, we have identified the members of this sample that are likely to be late type, nearby, or metal poor. We have performed optical and near-infrared spectroscopy on 41 objects, from which we measure spectral types that range from M4–T2.5. This sample includes 11 blue L dwarfs and five subdwarfs; the latter were also classified as such in the recent study by Kirkpatrick and coworkers. Based on their spectral types and photometry, several of our spectroscopic targets may have distances of < 20 pc with the closest at ~ 12 pc. The tangential velocities implied by the spectrophotometric distances and proper motions indicate that four of the five subdwarfs are probably members of the Galactic halo while several other objects, including the early-T dwarf WISE J210529.08–623558.7, may belong to the thick disk.

Subject headings: brown dwarfs — infrared: stars — proper motions — solar neighborhood — stars: low-mass

1. INTRODUCTION

Proper motions have long been used to identify members of the solar neighborhood. Measurements at optical wavelengths have been sensitive to stellar masses (Barnard 1916; Wolf 1919; Ross 1926; van Biesbroeck 1944; Giclas et al. 1971; Luyten 1979; Salim & Gould 2003; Hambly et al. 2004; Lépine et al. 2002, 2003; Lépine & Shara 2005; Lépine 2008; Subasavage et al. 2005; Boyd et al. 2011; Finch et al. 2012) while data in near-infrared (IR) bands have reached substellar objects (Artigau et al. 2006, 2010; Deacon et al. 2005, 2009, 2011; Deacon & Hambly 2007; Scholz et al. 2009; Scholz 2010; Sheppard & Cushing 2009; Kirkpatrick et al. 2010; Smith et al. 2014). The near-IR proper motion surveys have been enabled primarily by the Two Micron All-Sky Survey (2MASS, Skrutskie et al. 2006), the Deep Near-Infrared Survey of the Southern Sky (DENIS, Epchtein et al. 1999), the Sloan Digital Sky Survey (SDSS, York et al. 2000), the United Kingdom Infrared Telescope Infrared Deep Sky Survey (UKIDSS, Lawrence et al. 2007), and Pan-STARRS1 (Kaiser et al. 2002).

In 2010, the imaging available for proper motion surveys was extended to mid-IR wavelengths by the *Wide-field Infrared Survey Explorer (WISE)*, Wright et al. (2010). Proper motions have been measured by combining the *WISE* astrometry with optical and near-IR catalogs (Liu et al. 2011; Scholz et al. 2011, 2012; Gizis et al.

2011a,b, 2012; Castro & Gizis 2012; Castro et al. 2013; Bihain et al. 2013) and by employing only the multiple epochs of data obtained by *WISE* (Luhman 2013, 2014a; Thompson et al. 2013; Wright et al. 2014; Kirkpatrick et al. 2014). In one of the latter surveys, Luhman (2014a) searched for a distant companion to the Sun via the large parallactic motion that it would exhibit. During the course of that study, several hundred new high proper motion objects were found. In this paper, we investigate the nature of those objects by using photometry and proper motions from 2MASS and *WISE* to identify the ones that are likely to be late type, nearby, or metal poor (Section 2). We then use spectroscopy (Section 3) and kinematics (Section 4) to characterize in more detail a subset of that sample, focusing on the most promising candidates for L/T dwarfs and subdwarfs.

2. PHOTOMETRIC ANALYSIS

2.1. *Sample of High Proper Motion Objects*

Luhman (2014a) used multi-epoch astrometry from *WISE* to identify 762 high proper motion objects⁵. For this study, we consider the 761 sources that were detected by 2MASS because our analysis relies on both 2MASS and *WISE* photometry. The one remaining object that is absent from 2MASS, WISE J085510.83–071442.5, has been characterized by Luhman (2014b). We also examine an additional 20 high proper motion objects that are presented in Table 1, one of which (WISE J175510.28+180320.2) has already been reported by Griffith et al. (2012) and Mace et al. (2013a). These objects did not satisfy the criterion of $\mu/\sigma_\mu > 5$ for inclusion in the sample from Luhman (2014a), but they did exceed that threshold in an early version of the survey

¹ Based on data from the *Wide-field Infrared Survey Explorer*, the Two Micron All-Sky Survey, the NASA Infrared Telescope Facility, Gemini Observatory, the SOAR Telescope, and the Magellan Telescopes.

² Department of Astronomy and Astrophysics, The Pennsylvania State University, University Park, PA 16802, USA; kluhman@astro.psu.edu

³ Center for Exoplanets and Habitable Worlds, The Pennsylvania State University, University Park, PA 16802, USA

⁴ Department of Terrestrial Magnetism, Carnegie Institution of Washington, 5241 Broad Branch Rd. NW, Washington, DC 20015, USA

⁵ The sample from Luhman (2014a) was intended to contain only new high proper motion objects. However, Luhman (2014a) overlooked the proper motion survey by Pokorný et al. (2004), who had already identified 102 of the 762 objects presented by Luhman (2014a).

by Luhman (2014a) that used the preliminary release of data for the Post-Cryo phase, and at that stage they were confirmed as high proper motion stars using detections from 2MASS. Although all of these 20 sources appear in 2MASS images, some of them lack entries in the 2MASS Point Source Catalog, as noted in Table 1.

Kirkpatrick et al. (2014) have also performed a search for high proper motion objects with data from *WISE*, arriving at a sample of 3525 sources with motions confirmed by detections in other surveys like 2MASS. They described the overlap between their sample and the one from Luhman (2014a) and compared the distributions of magnitudes and proper motions between the two samples. We make one additional comment regarding that comparison. As illustrated in Figure 22 from Kirkpatrick et al. (2014), most of the stars that are in Kirkpatrick et al. (2014) but not in Luhman (2014a) have motions of $\lesssim 0''.3 \text{ yr}^{-1}$. This difference is a reflection of the fact that Luhman (2014a) excluded *WISE* sources with 2MASS counterparts within $3''$, which corresponds to $\mu \lesssim 0''.3 \text{ yr}^{-1}$, in order to focus on objects with larger motions, particularly those moving fast enough to be companions of the Sun ($\gtrsim 4'' \text{ yr}^{-1}$).

2.2. Common Proper Motion Companions

In Luhman (2014a), the 2MASS counterpart of *WISE* J163348.95–680851.6 was identified as 2MASS J16334908–6808480. However, upon closer inspection of the images from 2MASS, *WISE*, and the Digitized Sky Survey, we find that the *WISE* source is a blend of 2MASS J16334908–6808480 and a slightly fainter comoving star, 2MASS J16334976–6808488. As a result, the proper motion reported for this pair by Luhman (2014a) is incorrect. Using the astrometry for the blend from *WISE* and the mean coordinates of the pair from 2MASS, we measure $(\mu_\alpha \cos \delta, \mu_\delta) = (-0.27 \pm 0.02'' \text{ yr}^{-1}, -0.32 \pm 0.02'' \text{ yr}^{-1})$. The angular separation of the pair is $3''.9$, corresponding to 40–50 AU for the spectrophotometric distance estimated in Section 4.

We have attempted to identify additional common proper motion companions in the samples from Luhman (2014a) and Table 1. For each member of those samples, we searched for stars at separations of $\Delta\theta \leq 10'$ that have a similar proper motion ($\Delta\mu \lesssim 0.05'' \text{ yr}^{-1}$) in a catalog of previously known high proper motion objects that was compiled for the study by Luhman (2014a). The resulting common proper motion pairs are listed in Table 2, all of which satisfy the companionship criterion of $\Delta\theta\Delta\mu < (\mu/0.15)^{3.8}$ proposed by Lépine & Bongiorno (2007).

2.3. Identifying Late-type Objects

The spectral types of the objects in our proper motion sample can be estimated from their 2MASS and *WISE* colors. In Figure 1, we plot $J - W2$ versus $W1 - W2$ and $J - H$ versus $H - K_s$ for the sample. The colors are indicative of spectral types ranging from K through mid-T. To illustrate more precisely how the objects are distributed with spectral type, we include in Figure 1 polynomial fits to the mean colors of K dwarfs from SIMBAD and M0–T4 dwarfs from Leggett et al. (2010) and Kirkpatrick et al. (2011, 2012). The parameters that define these fits are presented in Table 3.

We also show the sample of L subdwarfs compiled by Kirkpatrick et al. (2010), which are significantly bluer than normal L dwarfs in $J - W2$, $J - H$, and $H - K_s$. According to Figure 1, most of the high proper motion objects are probably M dwarfs. They are slightly bluer on average in $J - H$ and $H - K_s$ than the fit to normal M dwarfs, which may indicate subsolar metallicities. The sample also appears to contain a few dozen L dwarfs and several T dwarfs.

For each object in our sample, we have identified the closest point along the sequence of mean colors of normal dwarfs in $J - W2$ versus $W1 - W2$. The spectral types that correspond to those points are listed in Table 4. The colors $J - H$ and $H - K_s$ were excluded from this process because of their degeneracies with spectral type, as illustrated in Figure 1. Of course, these spectral types estimated from colors should be used primarily for selecting targets of spectroscopy, and should not be treated as true spectral types. Because subdwarfs are bluer than normal dwarfs in $J - W2$, their color-derived spectral types will be too early. Nevertheless, cool subdwarfs appear at locations in a diagram in the next section that are distinctive from those of most other high proper motion stars, which facilitates their selection for spectroscopy.

2.4. Identifying Nearby and Metal-poor Objects

We can estimate the distances of our high proper motion objects with a diagram of $W2$ versus the color-based spectral types, as shown in Figure 2. For comparison, we include a fit to absolute magnitude in $W2$, M_{W2} , as a function of spectral type for M6–T4 dwarfs from Dupuy & Liu (2012) and a fit to M_{W2} that we have derived for M2–M6 dwarfs from SIMBAD. These fits are shown for distances of 10 and 20 pc. Two objects are above the fit at 10 pc. The brighter one is *WISE* J104915.57–531906.1, which has a parallactic distance of 2.0 pc (Luhman 2013). The other source, *WISE* J163348.95–680851.6, appears to be an early L dwarf at ~ 6 pc based on Figure 2. However, it is an unresolved binary in the *WISE* images (Section 2.2) and the color-based spectral type is earlier than the spectroscopic classification of M8+M8.5 (Section 3), resulting in an underestimate of the distance. In Section 4, we estimate spectrophotometric distances of ~ 12 pc for the components of this pair. The color-magnitude diagram in Figure 2 implies distances of ~ 10 –100 pc for the remainder of the sample.

Because older stellar populations in the Galaxy have higher velocity dispersions and tend to have lower metallicities, metal-poor stars (subdwarfs) typically exhibit large values of reduced proper motion, which is defined as $H_m = m + 5\log(\mu) + 5$ (Luyten 1925) where m is a particular photometric band. Diagrams of reduced proper motion versus color or spectral type have been used previously to identify candidates for cool subdwarfs among high proper motion stars (Kirkpatrick et al. 2010, 2014) and to characterize the kinematics of known late-type dwarfs (Pinfield et al. 2014). We have calculated H_{W2} for the members of our proper motion sample. The resulting values are presented in Table 4 and are plotted versus the color-based types in Figure 2. We also include in Figure 2 the known L subdwarfs compiled by Kirkpatrick et al. (2010) using spectral types estimated from $J - W2$ and $W1 - W2$ in the man-

ner applied to our sample. Because of their blue colors, the color-based spectral types for these known subdwarfs are earlier than their true types. One of the L subdwarfs, SDSS J141624.08+134826.7 (Schmidt et al. 2010a; Bowler et al. 2010), has a small value of H_{W2} , but the others reside near the bottom of the reduced proper motion diagram in Figure 2, as expected (two are not plotted because they are below the lower limit). Several objects in our proper motion sample also appear in that same area of the diagram, and thus are promising candidates for cool subdwarfs.

3. SPECTROSCOPIC ANALYSIS

3.1. Spectroscopic Sample

We have obtained spectra of a subset of our sample of high proper motion objects to measure their spectral types, focusing on those that appear to have smaller distances, cooler temperatures, or lower metallicities based on the analysis of photometry and proper motions in Section 2. We have previously presented optical spectroscopy for the primary in the binary WISE J104915.57–531906.1 (Luhman 2013) and near-IR spectroscopy for both components (Burgasser et al. 2013). That system is included among the objects marked as spectroscopic targets in Figures 1 and 2. Table 5 lists the 41 additional objects that we have observed in this study (42 if the components of WISE J163348.95–680851.6 are counted separately). Eight of our targets were also classified spectroscopically by Mace et al. (2013a) and Kirkpatrick et al. (2014), as indicated in Table 5.

3.2. SOAR/Goodman

Six stars were observed with optical spectroscopy using the Goodman High Throughput Spectrograph at the Southern Astrophysical Research (SOAR) Telescope on the nights of 2013 June 2 and 2013 August 1. The instrument was operated with the 400 l/mm grating in second order, the GG445 filter, and the 0".84 slit, which produced a wavelength coverage of 5400–9400 Å and a resolution of 5 Å. The spectra were reduced using tasks within IRAF. For the observations with SOAR and all of the other instruments in this study, the slit was aligned near the parallactic angle for each target.

3.3. IRTF/SpeX

We obtained near-IR spectra of 22 objects with SpeX (Rayner et al. 2003) at the NASA Infrared Telescope Facility (IRTF) on the nights of January 3, June 18–20, August 25 and 26, and December 26 and 28 in 2013. One of the SOAR targets, WISE J194128.98–342335.8, was also observed again with SpeX because no other suitable targets were available at that time. The data were collected in the prism mode with a 0".8 slit (0.8–2.5 μm , $R = 150$), reduced with the Spextool package (Cushing et al. 2004), and corrected for telluric absorption (Vacca et al. 2003).

3.4. Magellan/FIRE

We performed near-IR spectroscopy on 12 targets with the Folded-Port Infrared Echellette (FIRE; Simcoe et al. 2013) at the Magellan 6.5 m Baade Telescope at Las Campanas Observatory on the nights of August 9 and 10 and October 27 and 28 in 2013. We used the prism

mode and the 0".6 slit. The resulting data extended from 0.8–2.5 μm and exhibited $R = 500$ –300 across this range. The data were reduced with the FIREHOSE pipeline, which includes modified versions of routines from Spextool.

3.5. Gemini/FLAMINGOS-2

One of our targets, WISE J210529.08–623558.7, was observed with FLAMINGOS-2 (Eikenberry et al. 2006) at the Gemini South telescope on the night of 2013 December 23. Long-slit spectroscopy was performed with the JH grism and the 1".08 slit, which produced data from 0.9–1.8 μm with $R = 200$ –400. Eight 140 sec exposures were collected in an ABBA dither pattern along the slit. The spectra were reduced with tasks in IRAF.

3.6. SOAR/OSIRIS

We obtained near-IR spectra of the components of WISE J163348.95–680851.6 with the Ohio State Infrared Imager/Spectrometer at SOAR on the night of 2014 January 31. We used the XD grism and the 1" slit, providing data from 1.2–2.35 μm with $R = 1400$. For each of the two stars, which were well-resolved, we collected eight 30 sec exposures. The data were reduced with IRAF.

3.7. Spectral Classification

Our optical spectra are presented in Figure 3. They exhibit the strong absorption bands from TiO and VO that are indicative of M spectral types. To classify these data, we compared them to spectra of M dwarf standards (Kirkpatrick et al. 1991; Henry et al. 1994). Each of our targets is well-matched by a dwarf standard. None were expected to be subdwarfs based on the reduced proper motion diagram in Figure 2. The resulting spectral types are presented in Table 5. The uncertainties are ± 0.5 subclass.

The near-IR spectra of our targets are shown in Figures 4–7. The spectra from FLAMINGOS-2 and OSIRIS have been smoothed to the resolution of the SpeX data. We have omitted data at wavelengths where the correction for telluric absorption was poor. To measure spectral types from these data, we compared them to spectra from the SpeX Prism Spectral Libraries for the dwarf standards adopted by Kirkpatrick et al. (2010). If a good match was found, we included the spectrum of the matching standard in Figures 4–7 and adopted its type. For the targets that did not agree with any of the dwarf standards, we were able to find a reasonably close match within the full sample of cool dwarfs in the Prism Libraries, which includes subdwarfs and various objects with peculiar spectra. Those matching spectra, and the dwarf standards with the same subclasses, are plotted with the targets in Figures 4–7. The spectral types derived through this process are listed in Table 5. They have uncertainties of ± 1 subclass unless indicated otherwise.

3.8. Comments on Individual Sources

For the targets that lacked a good match among the dwarf standards, we discuss their classifications in more detail below:

WISE J222409.64–185242.1. It closely resembles 2MASS J15201746–1755307, which has an IR spectral type of M8 (Kirkpatrick et al. 2010). It has deeper H₂O bands and a more triangular *H*-band spectrum than the M8V standard vB 10.

WISE J194128.98–342335.8 and *WISE J235408.36+551854.5*. They have similar spectra except that the former is slightly bluer. They are well-matched by an average of 2MASS J15561873+1300527 and 2MASS J01151621+3130061, for which Bowler et al. (2009) adopted d/sdM8 from the SpeX Prism Spectral Libraries. A good match is also provided by 2MASS J18284076+1229207 (M7.5 pec, Kirkpatrick et al. 2010).

WISE J001450.14–083823.1, *WISE J204027.24+695923.7*, *WISE J030601.64–033058.4*, and *WISE J043535.80+211509.2*. The spectra of these objects are similar except that the first two are bluer at $<1.3 \mu\text{m}$ and redder at $>1.3 \mu\text{m}$. The first two objects agree closely with 2MASS J16403197+1231068, which has optical classifications of sdM9 (Gizis & Harvin 2006) and d/sdM9 (Burgasser et al. 2007a). We adopt a type of sdM9 for all four objects, although a slightly later type may be more appropriate for latter pair. It is difficult to assess this possibility since late-M and early-L subclasses for subdwarfs are sparsely sampled by available IR spectra. Kirkpatrick et al. (2014) has reported optical types of sdL0 for all four objects and IR types of sdL0 for *WISE J030601.64–033058.4* and *WISE J043535.80+211509.2*.

WISE J174336.62+154901.3. It resembles 2MASS J14403186–1303263 (L1 pec, Kirkpatrick et al. 2010) except that its *K* band is more suppressed. It is bluer than the L1 dwarf standard 2MASS J21304464–0845205 at $>1.3 \mu\text{m}$.

WISE J232219.45–140726.2, *WISE J030845.36+325923.1*, *WISE J000131.93–084126.9*, and *WISE J203751.31–421645.2*. Their spectra are similar except that they become slightly bluer from the first to the last. In addition, *WISE J203751.31–421645.2* exhibits stronger absorption in the lines of FeH, Na I, and K I between 0.95– $1.3 \mu\text{m}$ than the others. These objects are best matched by 2MASS J17561080+2815238 (L1 pec, Kirkpatrick et al. 2010) and have deeper H₂O absorption and a bluer slope at $>1.3 \mu\text{m}$ than the L1 dwarf standard 2MASS J21304464–0845205.

WISE J195311.04–022954.7. Its spectrum is well-matched by that of 2MASS J09211410–2104446, which has an optical type of L1.5 (Reid et al. 2008) and an IR type of L4: (Burgasser et al. 2008a). It is bluer than the L2 dwarf standard Kelu 1.

WISE J103602.80+030615.6. It is roughly similar to 2MASS J00361617+1821104, which has optical and IR types of L3.5 and L4, respectively (Kirkpatrick et al. 2000; Burgasser et al. 2010). It is bluer at $>1.3 \mu\text{m}$ than the L4 dwarf standard 2MASS J21580457–1550098.

WISE J000622.67–131955.2. It broadly matches the L5 dwarf standard SDSS J083506.16+195304.4, but the *H*-band continuum exhibits a distinctive shape that may indicate the presence of an unresolved binary. For comparison, we include in Figure 6 the spectrum of 2MASS J17114573+2232044, whose spectrum was modeled as a L5+T5.5 binary (Burgasser et al. 2010).

WISE J095729.41+462413.5. It closely resembles 2MASS J08202996+4500315 (L5, Kirkpatrick et al.

2000) and is redder at $>1.3 \mu\text{m}$ than the L5 dwarf standard SDSS J083506.16+195304.4.

WISE J214155.85–511853.1. Its H₂O bands and spectral slope agree well with those of 2MASS J11181292–0856106 (L6 pec, Kirkpatrick et al. 2010), although its lines from FeH, Na I, and K I between 0.95– $1.3 \mu\text{m}$ are stronger. It is bluer at $>1.3 \mu\text{m}$ than the L6 dwarf standard 2MASS J10101480–0406499.

WISE J134310.44–121628.8. It is well-matched by 2MASS J11263991–5003550 (L6.5 pec, Burgasser et al. 2008a) and is bluer at $>1.3 \mu\text{m}$ than the L6 dwarf standard 2MASS J10101480–0406499.

WISE J005757.63+201304.2. The best available match is 2MASS J11582077+0435014 (sdL7, Kirkpatrick et al. 2010). Because the *H* and *K* bands are not quite as suppressed in *WISE J005757.63+201304.2*, we consider the classification of this object as a subdwarf to be tentative based on our data. However, Kirkpatrick et al. (2014) do classify it as sdL7 using optical and near-IR spectra.

WISE J193430.11–421444.3 and *WISE J004713.80–371033.3*. They are similar to SDSS J133148.92–011651.4, which has been classified as L6, L8, and T0 (Hawley et al. 2002; Knapp et al. 2004; Schneider et al. 2014). Among the dwarf standards in that range, L9 (DENIS-P J0255–4700) and T0 (SDSS J120747.17+024424.8) provide the better matches. The $>1.3 \mu\text{m}$ slopes of the two targets agree better with that of the T0 standard, but they do not show the *K*-band CH₄ absorption of the latter. Therefore, we adopt a spectral type of L9 for these two objects.

WISE J175510.28+180320.2. Except for small differences in the *K* band, it agrees well with SDSS J090900.73+652527.2, which has been modeled as an unresolved T1.5+T2.5 binary (Burgasser et al. 2010). This object was originally discovered by Griffith et al. (2012) and Mace et al. (2013a), who classified it as T2.

4. KINEMATIC ANALYSIS

To examine the kinematic properties of our spectroscopic sample, we began by estimating the distance for each object from its photometry and the absolute magnitude expected for its spectral type. We have done this with data in the *H* band because M_H does not differ significantly between dwarfs and subdwarfs at a given M or L spectral type (Faherty et al. 2012). We adopted the values of M_H produced by the fit to M_H as a function of spectral type from Dupuy & Liu (2012). These spectrophotometric distances were then combined with the proper motions to estimate tangential velocities. The resulting distances and velocities are presented in Table 5. If an object is an unresolved binary, its distance and velocity will be underestimated in this analysis.

Several previous studies have characterized the kinematics of samples of cool dwarfs and subdwarfs. They have shown that cool dwarfs with bluer colors exhibit higher V_{tan} , and hence are likely to belong to older populations with lower metallicities (Faherty et al. 2009; Schmidt et al. 2010b). For instance, those measurements have produced $V_{tan}(\text{median}) \sim 30 \text{ km s}^{-1}$ and $\sigma_{tan} \sim 20 \text{ km s}^{-1}$ for normal L and T dwarfs (Faherty et al. 2012), $<V_{tan}> \sim 66 \text{ km s}^{-1}$ for blue L dwarfs (Kirkpatrick et al. 2010), and $V_{tan} \sim 200$ –

300 km s⁻¹ for M and L subdwarfs (Schilbach et al. 2009; Kirkpatrick et al. 2010; Faherty et al. 2012). In our sample, 27 M/L dwarfs have $J - K_s$ colors that are > 0.1 mag bluer than the fit to normal dwarfs from Table 3; they exhibit $V_{tan}(\text{median}) = 122$ km s⁻¹. The remaining 12 M/L dwarfs with normal or red colors have $V_{tan}(\text{median}) = 68$ km s⁻¹. In addition, we derive $V_{tan}(\text{median}) = 90$ km s⁻¹ for our 11 blue L dwarfs and $V_{tan} = 300\text{--}400$ km s⁻¹ for our four sdM9 stars. Thus, we find similar kinematic trends as in the previous samples.

Our estimates of tangential velocities provide a rough indication of whether any of the objects in our sample might belong to the thick disk or halo of the Galaxy. Based on the simulated velocities exhibited by these populations from Dupuy & Liu (2012), it is likely that the four sdM9 stars are members of the halo. In addition, several objects have velocities that are suggestive of membership in the thick disk ($V_{tan} \sim 150\text{--}200$ km s⁻¹), one of which is the T1.5 dwarf WISE J210529.08–623558.7. It was the most promising candidate for a thick disk/halo T dwarf prior to spectroscopy, appearing in the lower right corner of the reduced proper motion diagram in Figure 2. To examine the spectrum of WISE J210529.08–623558.7 for evidence of low metallicity, we have included in Figure 7 the model spectra for early T dwarfs with metallicities of $[Fe/H] = 0$ and $[Fe/H] = -0.5$ ($T_{eff} = 1400$ K, $\log g = 5$, Burrows et al. 2006). The H -band spectra differ significantly between the two models while the observed spectrum of WISE J210529.08–623558.7 is similar to that of the dwarf standard. Although these data do not show an obvious signature of low metallicity, it would be worthwhile to pursue K -band spectroscopy to check for the suppression in that band that is characteristic of cool subdwarfs. To date, only a small number of T-type objects have been found that exhibit both kinematic and spectroscopic evidence of membership in the thick disk or halo (Mace et al. 2013b; Pinfield et al. 2014; Burningham et al. 2014).

5. DISCUSSION

We have analyzed a sample of 781 high proper motion objects found with multi-epoch astrometry from *WISE* (Table 1; Luhman 2014a). Using 2MASS and *WISE* photometry and proper motions, we have identified the members of this sample that are most likely to be nearby, cool, or metal poor. We have obtained spectra of 41 of these objects, arriving at spectral types of M4–T2.5. Our spectroscopic sample includes 11 blue L dwarfs and five subdwarfs. All of the latter were independently found as high proper motion objects and classified as subdwarfs by Kirkpatrick et al. (2014). Two of our candidate subdwarfs that we did not observe spectroscopically, WISE J070720.48+170533.0 and WISE J020201.24–313644.7, have been confirmed as such through spectra collected by Wright et al. (2014) and Kirkpatrick et al. (2014). The most promising remaining candidate subdwarf from our sample that lacks spectroscopy is WISE J141143.25–452418.3.

We have estimated spectrophotometric distances and tangential velocities for the members of our spectroscopic sample. The closest system appears to have a distance of ~ 12 pc, and several others may have distances within 20 pc. A few objects that lack spectra also may fall within 20 pc, as shown in Figure 2. Assuming that previous samples of high proper motion stars have been thoroughly searched for nearby stars, our proper motion survey and that of Kirkpatrick et al. (2014) imply that the current census of neighbors within 10 pc has a high level of completeness for spectral types of T and earlier. The tangential velocities in our sample are higher for bluer near-IR colors, which is the same trend found in previous studies. Four of the five subdwarfs exhibit velocities of $300\text{--}400$ km s⁻¹, which are indicative of membership in the Galactic halo. Several additional objects have velocities that are suggestive of the thick disk ($V_{tan} \sim 150\text{--}200$ km s⁻¹), including the early-T dwarf WISE J210529.08–623558.7. More definitive characterizations of the kinematics of these candidate members of the halo and thick disk will require measurements of parallaxes and radial velocities.

K. L. acknowledges support from grant NNX12AI47G from the NASA Astrophysics Data Analysis Program. *WISE* is a joint project of the University of California, Los Angeles, and the Jet Propulsion Laboratory (JPL)/California Institute of Technology (Caltech), funded by NASA. 2MASS is a joint project of the University of Massachusetts and the Infrared Processing and Analysis Center (IPAC) at Caltech, funded by NASA and the National Science Foundation (NSF). The IRTF is operated by the University of Hawaii under cooperative agreement NNX-08AE38A with NASA. The Gemini data were obtained through program GS-2013B-DD-5. Gemini Observatory is operated by the Association of Universities for Research in Astronomy, Inc., under a cooperative agreement with the NSF on behalf of the Gemini partnership: the NSF (United States), the National Research Council (Canada), CONICYT (Chile), the Australian Research Council (Australia), Ministério da Ciência, Tecnologia e Inovação (Brazil) and Ministerio de Ciencia, Tecnología e Innovación Productiva (Argentina). The SOAR Telescope is a joint project of the Ministério da Ciência, Tecnologia, e Inovação (MCTI) da República Federativa do Brasil, the U.S. National Optical Astronomy Observatory (NOAO), the University of North Carolina at Chapel Hill, and Michigan State University. Cerro Tololo Inter-American Observatory and NOAO are operated by the Association of Universities for Research in Astronomy, under contract with the National Science Foundation. This work used data from the SpeX Prism Spectral Libraries (maintained by Adam Burgasser at <http://www.browndwarfs.org/spexprism>), the NASA/IPAC Infrared Science Archive (operated by JPL under contract with NASA), and SIMBAD database, operated at CDS, Strasbourg, France. The Center for Exoplanets and Habitable Worlds is supported by the Pennsylvania State University, the Eberly College of Science, and the Pennsylvania Space Grant Consortium.

REFERENCES

- Artigau, É., Doyon, R., Lafrenière, D., et al. 2006, *ApJ*, 651, L57
- Artigau, É., Radigan, J., Folkes, S., et al. 2010, *ApJ*, 718, L38

- Barnard, E. E. 1916, *AJ*, 29, 191
- Bihain, G., Scholz, R.-D., Storm, J., & Schnurr, O. 2013, *A&A*, 557, A43
- Bowler, B. P., Liu, M. C., & Dupuy, T. J. 2010, *ApJ*, 710, 45
- Boyd, M. R., Henry, T. J., Jao, W.-C., Subasavage, J. P., & Hambly, N. C. 2011, *AJ*, 142, 92
- Bowler, B. P., Liu, M. C., & Cushing, M. C. 2009, *ApJ*, 706, 1114
- Burgasser, A. J. 2007, *ApJ*, 659, 655
- Burgasser, A. J., Cruz, K. L., Cushing, M. C., et al. 2010, *ApJ*, 710, 1142
- Burgasser, A. J., Cruz, K. L., & Kirkpatrick, J. D. 2007a, *ApJ*, 657, 494
- Burgasser, A. J., Geballe, T. R., Leggett, S. K., Kirkpatrick, J. D., & Golimowski, D. A. 2006, *ApJ*, 637, 1067
- Burgasser, A. J., Liu, M. C., Ireland, M. J., Cruz, K. L., & Dupuy, T. J. 2008b, *ApJ*, 681, 579
- Burgasser, A. J., Looper, D. L., Kirkpatrick, J. D., Cruz, K. L., & Swift, B. J. 2008a, *ApJ*, 674, 451
- Burgasser, A. J., Looper, D. L., Kirkpatrick, J. D., & Liu, M. C. 2007b, *ApJ*, 658, 557
- Burgasser, A. J., & McElwain, M. W. 2006, *AJ*, 131, 1007
- Burgasser, A. J., McElwain, M. W., Kirkpatrick, J. D., et al. 2004, *AJ*, 127, 2856
- Burgasser, A. J., Sheppard, S. S., & Luhman, K. L. 2013, *ApJ*, 772, 129
- Burningham, B., Smith, L., Cardoso, C. V., et al. 2014, *MNRAS*, in press
- Burrows, A., Sudarsky, D., & Hubeny, I. 2006, *ApJ*, 640, 1063
- Castro, P. J., & Gizis, J. E. *ApJ*, 746, 3
- Castro, P. J., Gizis, J. E., Harris, H. C., et al. 2013, *ApJ*, 776, 126
- Chiu, K., Fan, X., Leggett, S. K., et al. 2006, *AJ*, 131, 2722
- Cruz, K. L., Burgasser, A. J., Reid, I. N., & Liebert, J. 2004, *ApJ*, 604, L61
- Cushing, M. C., Vacca, W. D., & Rayner, J. T. 2004, *PASP*, 116, 362
- Deacon, N. R., & Hambly, N. C. 2007, *A&A*, 468, 163
- Deacon, N. R., Hambly, N. C., & Cook, J. A. 2005, *A&A*, 435, 363
- Deacon, N. R., Hambly, N. C., King, R. R., & McCaughrean, M. J. 2009, *MNRAS*, 394, 857
- Deacon, N. R., Liu, M. C., Magnier, E. A., et al. 2011, *AJ*, 142, 77
- Dupuy, T. J., & Liu, M. C. 2012, *ApJS*, 201, 19
- Eikenberry, S., Elston, R., Raines, S. N., et al. 2006, *SPIE*, 6269, 39
- Epchtein, N., Deul, E., Derriere, S., et al. 1999, *A&A*, 349, 236
- Faherty, J. K., Burgasser, A. J., Cruz, K. L., et al. 2009, *AJ*, 137, 1
- Faherty, J. K., Burgasser, A. J., Walter, F. M., et al. 2012, *ApJ*, 752, 56
- Finch, C. T., Zacharias, N., Boyd, M. R., Henry, T. J., & Hambly, N. C. 2012, *ApJ*, 745, 118
- Giclas, H. L., Burnham, R., & Thomas, N. G. 1971, *The Lowell Proper Motion Survey (Flagstaff, AZ: Lowell Observatory)*
- Gizis, J. E., Burgasser, A. J., Faherty, J. K., Castro, P. J., & Shara, M. M. 2011b, *AJ*, 142, 171
- Gizis, J. E., Faherty, J. K., Liu, M. C., et al. 2012, *AJ*, 144, 94
- Gizis, J. E., & Harvin, J. 2006, *AJ*, 132, 2372
- Gizis, J. E., Troup, N. W., & Burgasser, A. J. 2011a, *ApJ*, 736, L34
- Griffith, R. L., Kirkpatrick, J. D., Eisenhardt, P. R. M., et al. 2012, *AJ*, 144, 148
- Hambly, N. C., Henry, T. J., Subasavage, J. P., Brown, M. A., & Jao, W. C. 2004, *AJ*, 128, 437
- Hawley, S. L., Covey, K. R., Knapp, G. R., et al. 2002, *AJ*, 123, 3409
- Henry, T. J., Kirkpatrick, J. D., & Simons, D. A. 1994, *AJ*, 108, 1437
- Kaiser, N., Aussel, H., Burke, B. E., et al. 2002, *Proc. SPIE*, 4836, 154
- Kirkpatrick, J. D., Cushing, M. C., Gelino, C. R., et al. 2011, *ApJS*, 197, 19
- Kirkpatrick, J. D., Gelino, C. R., Cushing, M. C., et al. 2012, *ApJ*, 753, 156
- Kirkpatrick, J. D., Henry, T. J., & McCarthy, D. W. 1991, *ApJS*, 77, 417
- Kirkpatrick, J. D., Looper, D. L., Burgasser, A. J., et al. 2010, *ApJS*, 190, 100
- Kirkpatrick, J. D., Reid, I. N., Liebert, J., et al. 2000, *AJ*, 120, 447
- Kirkpatrick, J. D., Schneider, A., Fajardo-Acosta, S., et al. 2014, *ApJ*, 783, 122
- Knapp, G. R., Leggett, S. K., Fan, X., et al. 2004, *AJ*, 127, 3553
- Lawrence, A., Warren, S. J., Almaini, O., et al. 2007, *MNRAS*, 379, 1599
- Leggett, S. K., Burningham, B., Saumon, D., et al. 2010, *ApJ*, 710, 1627
- Lépine, S. 2008, *AJ*, 135, 2177
- Lépine, S., & Bongiorno, B. 2007, *AJ*, 133, 899
- Lépine, S., & Shara, M. M. 2005, *AJ*, 129, 1483
- Lépine, S., Shara, M. M., Rich, R. M. 2002, *AJ*, 124, 1190
- Lépine, S., Shara, M. M., Rich, R. M. 2003, *AJ*, 126, 921
- Liu, M. C., Deacon, N. R., Magnier, E. A., et al. 2011, *ApJ*, 740, L32
- Looper, D. L., Kirkpatrick, J. D., & Burgasser, A. J. 2007, *AJ*, 134, 1162
- Luhman, K. L. 2013, *ApJ*, 767, L1
- Luhman, K. L. 2014a, *ApJ*, 781, 4
- Luhman, K. L. 2014b, *ApJ*, in press
- Luyten, W. J. 1925, *ApJ*, 62, 8
- Luyten, W. J. *LHS Catalogue. A Catalogue of Stars with Proper Motions Exceeding 0"5 annually*, 2nd edn. Univ. Minnesota, Minneapolis, MN
- Mace, G. N., Kirkpatrick, J. D., Cushing, M. C., et al. 2013, *ApJS*, 206, 6
- Mace, G. N., Kirkpatrick, J. D., Cushing, M. C., et al. 2013, *ApJ*, 777, 36
- Pinfield, D. J., Gomes, J., Day-Jones, A. C., et al. 2014, *MNRAS*, 437, 1009
- Pokorny, R. S., Jones, H. R. A., Hambly, N. C., & Pinfield, D. J. 2004, *A&A*, 421, 763
- Rayner, J. T., Toomey, D. W., Onaka, P. M., et al. 2003, *PASP*, 115, 362
- Reid, I. N., Cruz, K. L., Kirkpatrick, J. D., et al. 2006, *AJ*, 136, 1290
- Reid, I. N., Lewitus, E., Burgasser, A. J., & Cruz, K. L. 2006, *ApJ*, 639, 1114
- Ross, F. E. 1926, *AJ*, 36, 124
- Salim, A., & Gould, A. 2003, *ApJ*, 582, 1011
- Schilbach, E., Röser, S., & Scholz, R.-D. 2009, *A&A*, 493, L27
- Schmidt, S. J., West, A. A., Burgasser, A. J., Bochanski, J. J., & Hawley, S. L. 2010a, *AJ*, 139, 1045
- Schmidt, S. J., West, A. A., Hawley, S. L., & Pineda, J. S. 2010b, *AJ*, 139, 1808
- Schneider, A. C., Cushing, M. C., Kirkpatrick, J. D., et al. 2014, *AJ*, 147, 34
- Scholz, R.-D. 2010, *A&A*, 515, A92
- Scholz, R.-D., Bihain, G., Schnurr, O., & Storm, J. 2011, *A&A*, 532, L5
- Scholz, R.-D., Bihain, G., Schnurr, O., & Storm, J. 2012, *A&A*, 541, A163
- Scholz, R.-D., Storm, J., Knapp, G. R., & Zinnecker, H. 2009, *A&A*, 494, 949
- Sheppard, S. S., & Cushing, M. C. 2009, *AJ*, 137, 304
- Simcoe, R. A., Burgasser, A. J., Schechter, P. L., et al. 2013, *PASP*, 125, 270
- Skrutskie, M., Cutri, R. M., Stiening, R., et al. 2006, *AJ*, 131, 1163
- Smith, L., Lucas, P. W., Burningham, B., et al. 2014, *MNRAS*, 437, 3603
- Subasavage, J. P., Henry, T. J., Hambly, N. C., Brown, M. A., Jao, W.-C., & Finch, C. T. 2005, *AJ*, 130, 1658
- Thompson, M. A., Kirkpatrick, J. D., Mace, G. N., et al. 2013, *PASP*, 125, 809
- Vacca, W. D., Cushing, M. C., & Rayner, J. T., 2003, *PASP*, 115, 389
- van Biesbroeck, G. 1944, *AJ*, 51, 61
- Wolf, M. 1919, *Veröffentlichungen der Badischen Sternwarte zu Heidelberg*, 7, 195
- Wright, E. L., Eisenhardt, P. R. M., Mainzer, A. K., et al. 2010, *AJ*, 140, 1868
- Wright, E. L., Kirkpatrick, J. D., Gelino, C. R., et al. 2014, *AJ*, 147, 61
- York, D. G., Adelman, J., Anderson, J. E., et al. 2000, *AJ*, 120, 1579

TABLE 1
NEW HIGH PROPER MOTION OBJECTS

WISE	2MASS	$\mu_\alpha \cos \delta$ (arcsec yr ⁻¹)	μ_δ (arcsec yr ⁻¹)	J (mag)	H (mag)	K_s (mag)	W1 (mag)	W2 (mag)
J000131.93–084126.9	J00013166–0841234	0.331±0.014	–0.299±0.014	15.71±0.05	15.03±0.06	14.70±0.09	14.29±0.03	13.96±0.05
J020110.68–523916.9	J02011020–5239186	0.418±0.014	0.155±0.015	16.45±0.11	15.58±0.10	14.63±0.10	14.11±0.03	13.62±0.04
J030845.36+325923.1	J03084507+3259277	0.310±0.011	–0.376±0.012	15.80±0.06	15.19±0.07	14.71±0.07	14.48±0.03	14.14±0.06
J045425.37+400408.5	J04542499+4004106	0.386±0.011	–0.169±0.012	15.38±0.05	14.97±0.08	14.50±0.08	14.37±0.04	14.33±0.09
J060609.90–145318.3	...	0.136±0.010	–0.200±0.010	12.80±0.03	12.31±0.02	12.07±0.02	11.93±0.02	11.79±0.02
J061700.64+040050.0	J06170068+0400548	–0.057±0.010	–0.459±0.010	14.29±0.03	13.79±0.04	13.39±0.03	13.27±0.03	12.99±0.03
J080457.04–374622.1	J08045688–3746183	0.200±0.012	–0.331±0.010	14.69±0.03	14.15±0.04	13.73±0.05	13.47±0.03	13.18±0.03
J095729.41+462413.5	J09572983+4624177	–0.354±0.011	–0.353±0.011	16.25±0.11	15.37±0.13	14.45±0.09	13.68±0.03	13.41±0.04
J103602.80+030615.6	J10360307+0306160	–0.403±0.015	–0.043±0.014	15.97±0.10	15.48±0.11	14.82±0.12	14.35±0.03	14.03±0.05
J145209.23–423545.6	...	–0.260±0.010	–0.153±0.010	13.09±0.10 ^a	12.45±0.10 ^a	12.34±0.10 ^a	12.23±0.03	12.13±0.03
J151612.81–550826.5	...	–0.227±0.010	–0.144±0.010	13.99±0.03	13.45±0.03	13.30±0.04	13.23±0.03	13.22±0.03
J175510.28+180320.2	J17551062+1803203	–0.453±0.014	–0.008±0.014	16.02±0.09	15.22±0.09	14.68±0.13	14.60±0.03	13.73±0.04
J184936.22–204538.1	J18493649–2045352	–0.313±0.010	–0.247±0.010	13.83±0.03	13.30±0.03	13.05±0.04	12.97±0.03	12.80±0.04
J193430.11–421444.3	J19343030–4214401	–0.204±0.024	–0.397±0.025	16.79±0.17	15.67±0.16	15.29±0.17	14.81±0.04	14.45±0.07
J195311.04–022954.7	J19531118–0229501	–0.187±0.010	–0.403±0.012	15.64±0.05	14.86±0.07	14.45±0.07	14.01±0.03	13.62±0.04
J203644.55–084715.1	J20364425–0847138	0.379±0.010	–0.118±0.010	13.42±0.03	12.88±0.03	12.43±0.02	12.10±0.02	11.81±0.02
J203751.31–421645.2	J20375108–4216410	0.229±0.010	–0.391±0.010	15.50±0.05	14.76±0.06	14.27±0.06	13.96±0.03	13.71±0.04
J211157.85–521111.2	...	–0.237±0.031	0.095±0.032	16.56±0.17	15.92±0.21	...	15.36±0.05	14.25±0.05
J214152.86–145013.4	J21415277–1450092	0.115±0.011	–0.386±0.010	14.46±0.04	13.97±0.04	13.71±0.05	13.52±0.03	13.23±0.04
J232219.45–140726.2	J23221914–1407238	0.399±0.020	–0.221±0.019	15.99±0.07	15.52±0.11	15.10±0.14	14.68±0.04	14.31±0.06

NOTE. — J , H , and K_s are from the 2MASS Survey Point Source Reject Table for WISE J060609.90–145318.3, WISEA J151612.81–550826.5, and WISE J211157.85–521111.2. Our manual measurement of photometry from the 2MASS images for WISE J145209.23–423545.6, and from the 2MASS Point Source Catalog for all other sources. The AllWISE Source Catalog for WISEA J151612.81–550826.5 and from WISE All-Sky Source Catalog for all other sources. WISE detections that appear false upon visual inspection have been omitted. Proper motions are based on astrometry from 2MASS and WISE. The 2MASS astrometry for WISE J145209.23–423545.6 was not used from those images.

^a The high proper motion star is blended with an artifact in the 2MASS images, but it appears to be the dominant source of flux.

TABLE 2
COMMON PROPER MOTION PAIRS

New High Proper Motion Object	Known Star with Similar Proper Motion	Separation (arcsec)
WISE J035227.54–315104.9 ^a	LHS 1609	40
WISE J051723.87–345121.8 ^a	HD 34642	159
WISE J064837.92+073658.4	HD 49409	28
WISE J065717.78–144641.2	LP 721-15	43
WISE J111614.19–440325.2	LHS 2386	355
WISE J124014.80+204752.8 ^a	BD+21 2442	113
WISE J141420.38–055709.1	HD 124553	21
WISE J145824.02–390754.7	SCR J1457–3904	446
WISE J154803.74–581055.5	LHS 3119	21
WISE J190756.42–151416.3	HD 178140	22
WISE J191046.06–413348.7	2MASS J19103460–4133443	128
WISE J200436.76–712356.6	LTT 7914	39
WISE J202218.29–582110.3	WD 2018–585	65
WISE J222742.02–233733.4	LP 876-1	64

^a The common proper motion of this pair was previously noted by Kirkpatrick et al. (2014).

TABLE 3
COEFFICIENTS OF POLYNOMIAL FITS TO COLORS FOR DWARFS FROM K0–T4

y	c_0	c_1	c_2	c_3	c_4	c_5
$J - H$	0.5879725	-4.185039×10^{-4}	-8.971617×10^{-4}	3.156630×10^{-4}	1.088121×10^{-6}	-5.701197×10^{-7}
$H - K_s$	0.1943348	1.967872×10^{-2}	1.172085×10^{-3}	1.991087×10^{-5}	1.084605×10^{-7}	-2.049361×10^{-7}
$J - W2$	0.9256119	5.609014×10^{-2}	2.061348×10^{-3}	3.043627×10^{-4}	5.493171×10^{-5}	-9.495056×10^{-7}
$W1 - W2$	4.016049×10^{-2}	2.857693×10^{-2}	9.994479×10^{-4}	-1.337646×10^{-4}	-1.948121×10^{-6}	3.257249×10^{-7}

NOTE. — $y = \sum_{i=0}^5 c_i x^i$ where $x = -8, 0, 10$, and 20 for K0, M0, L0, and T0, respectively.

TABLE 4
REDUCED PROPER MOTIONS AND SPECTRAL TYPE
ESTIMATES

WISE	H_{W2}	Spectral Type Estimated from Colors ^a
J000131.93–084126.9	17.21	8.8
J000622.67–131955.2	17.18	16.4
J000721.39+500302.7	16.54	4.7
J001318.52–554802.3	16.79	6.5
J001450.14–083823.1	19.01	5.5

NOTE. — This table is available in its entirety in a machine-readable form in the online journal. A portion is shown here for guidance regarding its form and content.

^a Numerical types are defined such that -8 , 0 , 10 , and 20 correspond to K0, M0, L0, and T0, respectively.

TABLE 5
SPECTRAL TYPES, DISTANCES, AND TANGENTIAL VELOCITIES OF HIGH PROPER MOTION OBJECTS

WISE	Telescope/Instrument	Date	Spectral Type	Distance ^a (pc)	V_{tan} ^b (km/s)
J000131.93−084126.9	IRTF/SpeX	2013 Aug 26	L1 pec (blue)	61±13	129±29
J000622.67−131955.2	IRTF/SpeX	2013 Jan 3	L5 pec	41±9	95±21
J001450.14−083823.1	IRTF/SpeX	2013 Dec 28	sdM9 ^c	47±10	328±69
J002656.73−542854.8	SOAR/Goodman	2013 Aug 1	M8V	19±4	34±6
J004713.80−371033.3	Magellan/FIRE	2013 Oct 27	L9 pec (blue) ^d	23±4	64±11
J005757.63+201304.2	IRTF/SpeX	2013 Dec 28	sdL7? ^e	29±6	122±24
J011154.36−505343.2	Magellan/FIRE	2013 Oct 27	T1.5	17±2	40±5
J020110.68−523916.9	Magellan/FIRE	2013 Aug 9	L8.5	26±5	56±10
J030601.64−033058.4	IRTF/SpeX	2013 Dec 26	sdM9 ^c	49±10	307±65
J030845.36+325923.1	IRTF/SpeX	2013 Aug 26	L1 pec (blue)	65±15	151±34
J032301.86+562558.0	IRTF/SpeX	2013 Dec 26	L7	18±3	35±7
J042449.21−595905.6	Magellan/FIRE	2013 Oct 28	T0	28±4	40±6
J042949.41−783705.6	Magellan/FIRE	2013 Oct 28	L3±2	54±19	128±45
J043535.80+211509.2	IRTF/SpeX	2013 Dec 26	sdM9 ^c	66±14	398±84
J082000.48−662211.9	Magellan/FIRE	2013 Oct 28	L9.5	21±3	33±4
J082640.46−164032.0	Magellan/FIRE	2013 Oct 27	L9 ^f	16±3	75±13
J095729.41+462413.5	IRTF/SpeX	2013 Jun 18	L5 pec (red)	38±9	89±20
J103602.80+030615.6	IRTF/SpeX	2013 Jun 19	L4 pec (blue)	47±11	90±20
J131211.10−761740.9	Magellan/FIRE	2013 Aug 10	L5.5	33±7	87±19
J134310.44−121628.8	IRTF/SpeX	2013 Jun 19	L6.5±2 pec (blue)	31±10	68±21
J163348.95−680851.6	SOAR/OSIRIS	2014 Jan 31	M8V+M8.5V ^g	12±2	23±5
J172733.09−155414.2	IRTF/SpeX	2013 Jun 20	M4V	64±31	128±63
J174336.62+154901.3	IRTF/SpeX	2013 Jun 20	L1 pec (blue)	34±8	56±12
J175510.28+180320.2	IRTF/SpeX	2013 Jun 18	T2 ^h	19±2	40±5
J193430.11−421444.3	Magellan/FIRE	2013 Aug 9	L9 pec (blue)	26±5	56±10
J194128.98−342335.8	SOAR/Goodman	2013 Aug 1	M8.5V	50±9	143±26
J195311.04−022954.7	IRTF/SpeX	2013 Aug 25	M8 pec (blue)	53±12	152±34
J200907.88−170448.0	IRTF/SpeX	2013 Jun 19	L2 pec (blue)	49±11	102±24
J203644.55−084715.1	SOAR/Goodman	2013 Aug 1	M6V	103±24	330±78
J203751.31−421645.2	Magellan/FIRE	2013 Aug 9	M8.5V	30±6	57±11
J204027.24+695923.7	Magellan/FIRE	2013 Aug 9	L1 pec (blue)	54±12	115±26
J204027.24+695923.7	IRTF/SpeX	2013 Dec 28	sdM9 ^c	35±7	380±81
J210529.08−623558.7	Gemini/FLAMINGOS-2	2013 Dec 23	T1.5	26±4	176±25
J211157.85−521111.2	Magellan/FIRE	2013 Aug 9	T2.5	25±4	31±5
J211807.07−321713.5	IRTF/SpeX	2013 Aug 25	L1.5	46±10	80±18
J212354.78−365223.4	IRTF/SpeX	2013 Aug 25	L1.5	45±10	109±25
J212502.66−453353.5 ⁱ	SOAR/Goodman	2013 Aug 1	M4V	73±21	132±39
J214152.86−145013.4	SOAR/Goodman	2013 Aug 1	M5.5V	136±40	261±77
J214155.85−511853.1	Magellan/FIRE	2013 Aug 9	L6 pec (blue)	19±4	65±14
J222409.64−185242.1	IRTF/SpeX	2013 Aug 25	M8	52±12	96±21
J232219.45−140726.2	IRTF/SpeX	2013 Aug 25	L1 pec (blue)	76±17	165±37
J235408.36+551854.5	IRTF/SpeX	2013 Dec 26	M8 pec (blue)	31±7	196±44

^a Spectrophotometric distances based on the 2MASS H -band photometry and the value of M_H produced by the relation between spectral type and M_H from Dupuy & Liu (2012) except for the two stars classified as M4V, for which the median M_H for M4 dwarfs within 8 pc was used (Kirkpatrick et al. 2012).

^b Estimated from the spectrophotometric distances and the proper motions in Table 1 and Luhman (2014a).

^c Classified as sdL0 by Kirkpatrick et al. (2014).

^d Classified as L4: by Kirkpatrick et al. (2014).

^e Classified as sdL7 by Kirkpatrick et al. (2014).

^f Classified as L9 by Kirkpatrick et al. (2014).

^g The spectral types apply to the west and east components, respectively.

^h Classified as T2 by Mace et al. (2013a).

ⁱ Originally identified as a high proper motion star by Pokorný et al. (2004).

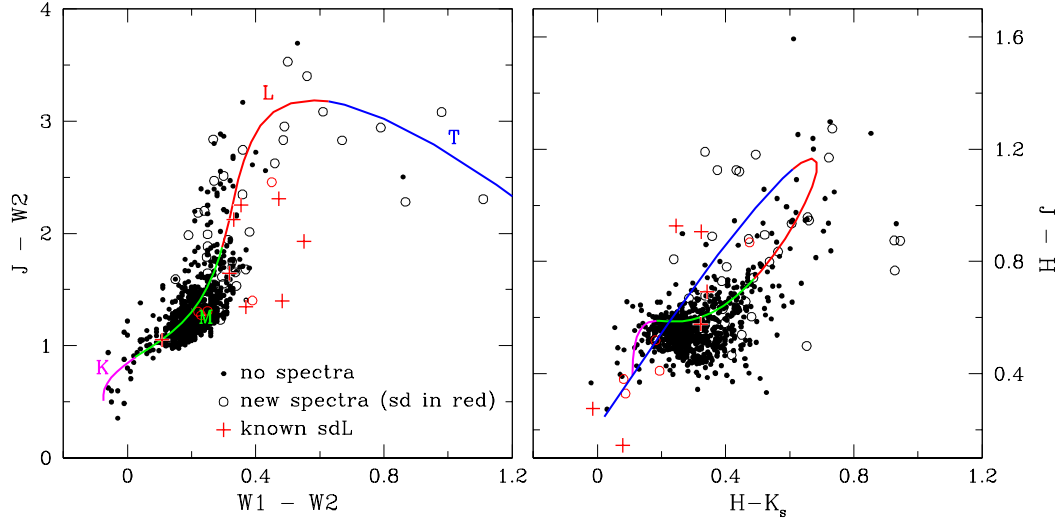


FIG. 1.— Color-color diagrams for high proper motion objects identified with *WISE* (Luhman 2014a, Table 1), which are marked according to whether we have obtained spectra of them (filled and open circles). The spectroscopic targets classified as subdwarfs are plotted in red. For comparison, we show fits to the median colors for known dwarfs from K0–T4 (solid lines, Table 3) and the colors of known L subdwarfs (crosses, Kirkpatrick et al. 2010, references therein). We have estimated spectral types for the high proper motion objects based on their proximity to the fits in $J - W2$ and $W1 - W2$, which are used in Figure 2.

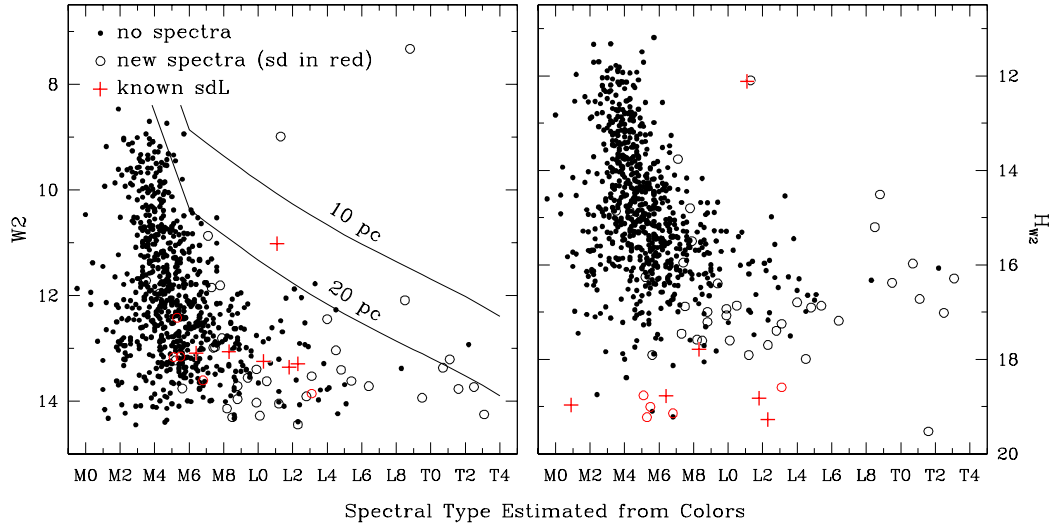


FIG. 2.— $W2$ and reduced proper motion in $W2$ (H_{W2}) versus the spectral type estimated from $J - W2$ and $W1 - W2$ (Figure 1) for high proper motion objects identified with *WISE* (filled and open circles). In the left panel, a fit to M_{W2} as a function of spectral type is shown for 10 and 20 pc (solid lines, Section 2.4, Dupuy & Liu 2012).

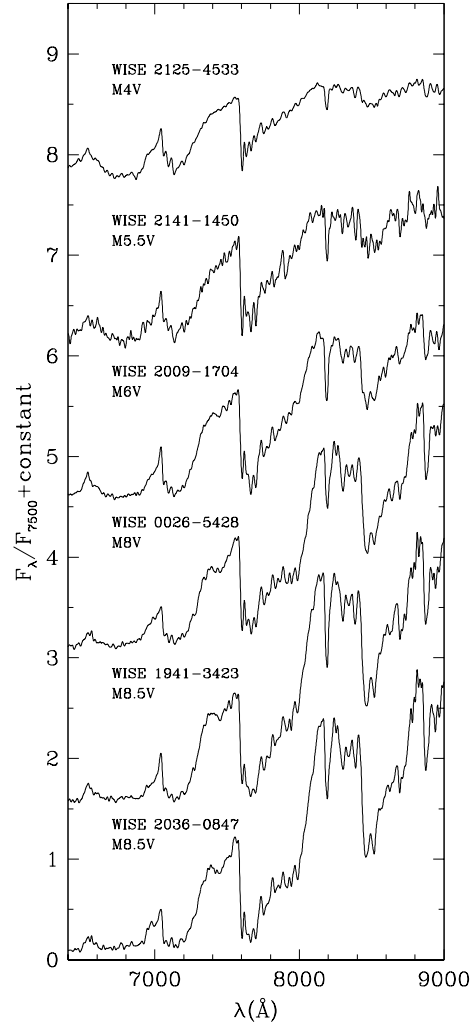


FIG. 3.— Optical spectra of high proper motion objects found with *WISE*. The spectral types measured from these data are indicated. The data are displayed at a resolution of 13 \AA and are normalized at 7500 \AA .

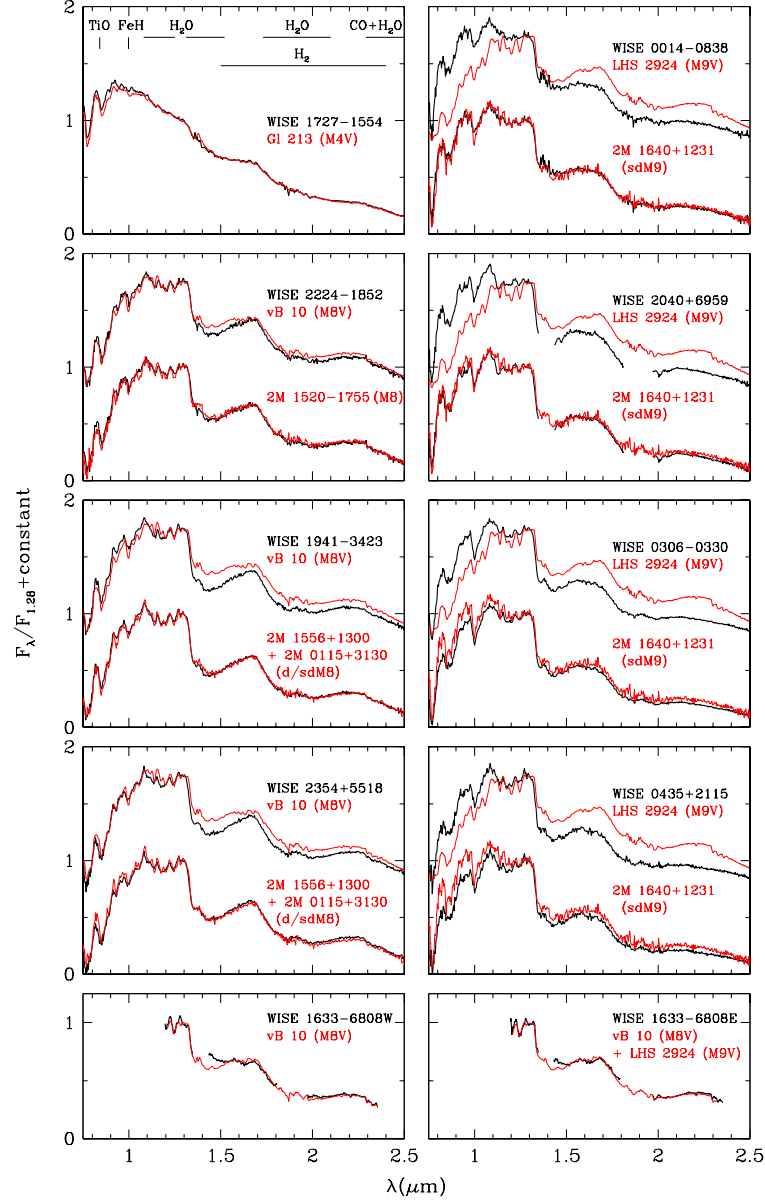


FIG. 4.— Near-IR spectra of high proper motion objects found with *WISE* (black spectra). Each spectrum is compared to data for a dwarf standard and, in some cases, data for another object that provide a better match (upper and lower red spectra). The comparison spectra are from Burgasser et al. (2004), Burgasser & McElwain (2006), Kirkpatrick et al. (2010), and our unpublished observations.

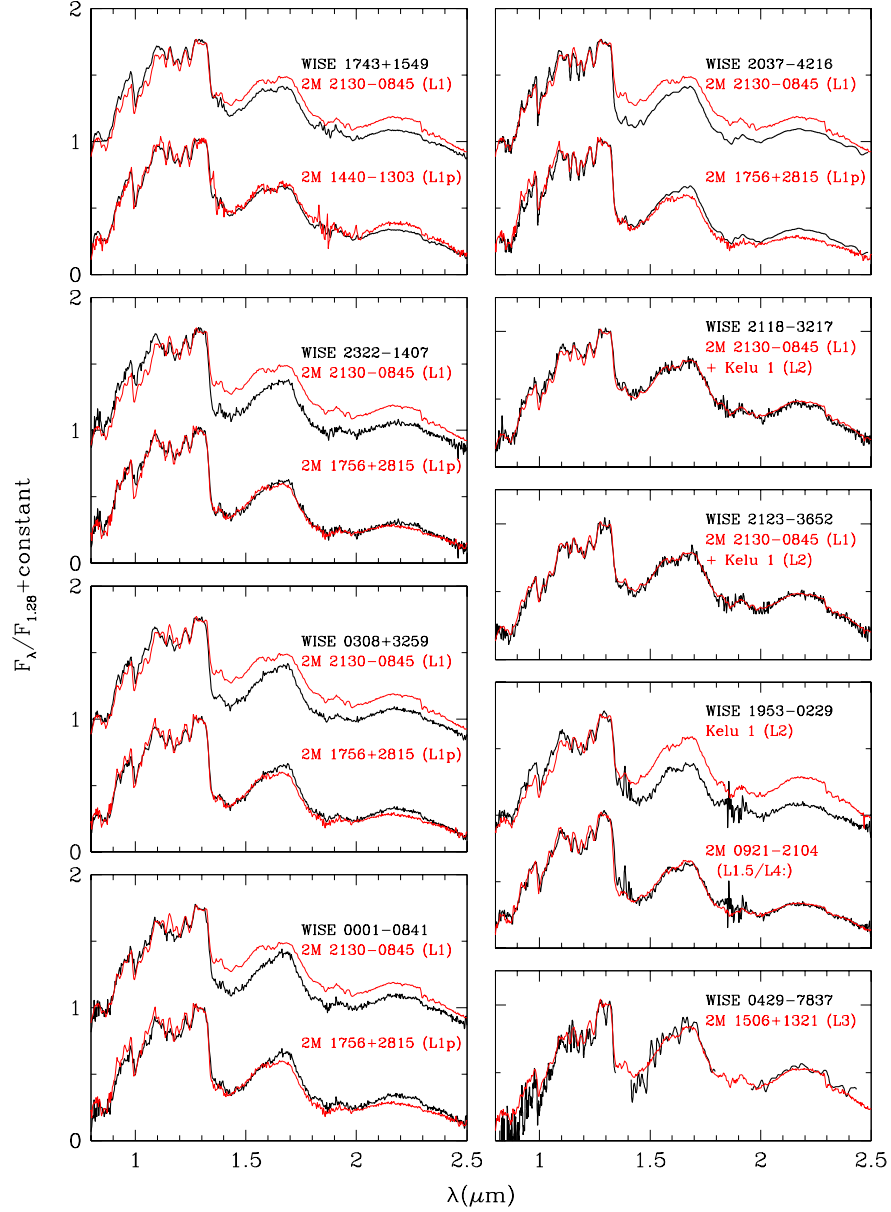


FIG. 5.— More near-IR spectra of high proper motion objects found with *WISE* (see Fig. 4). The comparison spectra are from Burgasser (2007), Burgasser et al. (2007b), and Kirkpatrick et al. (2010).

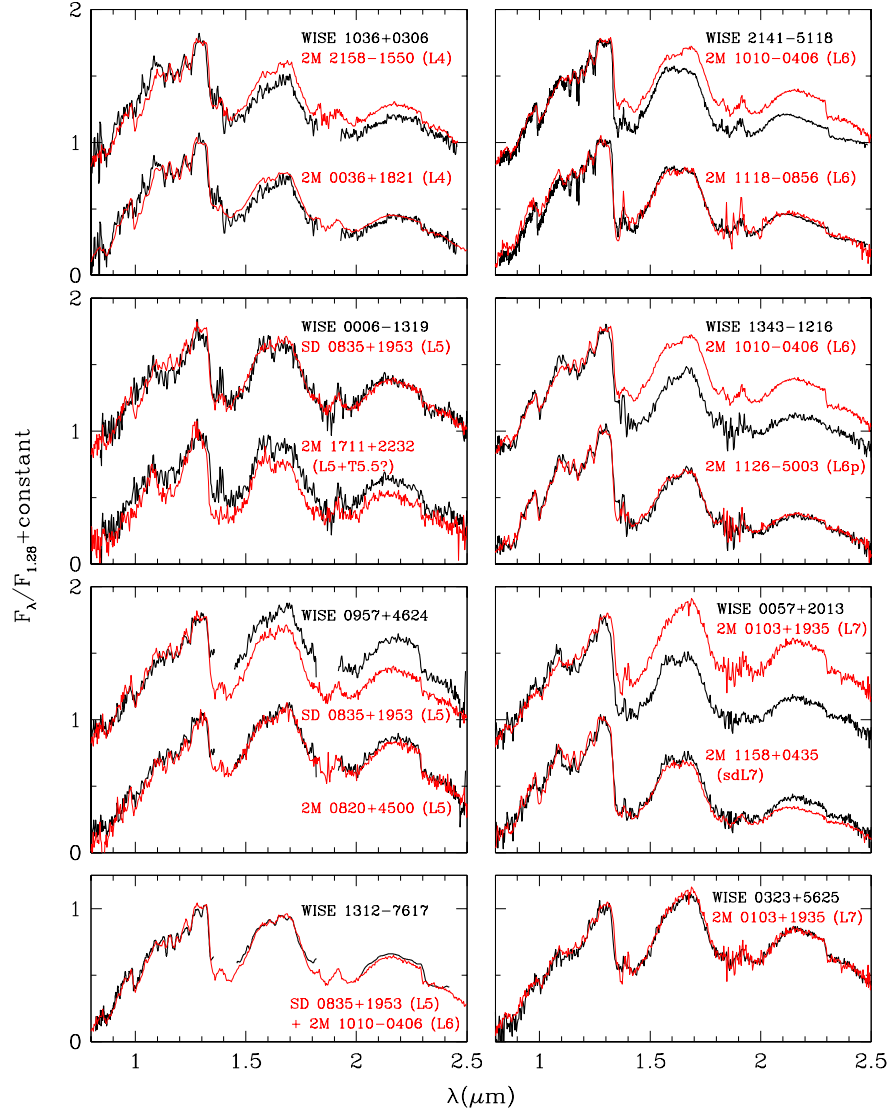


FIG. 6.— More near-IR spectra of high proper motion objects found with *WISE* (see Fig. 4). The comparison spectra are from Cruz et al. (2004), Chiu et al. (2006), Reid et al. (2006), Burgasser et al. (2008b, 2010), and Kirkpatrick et al. (2010).

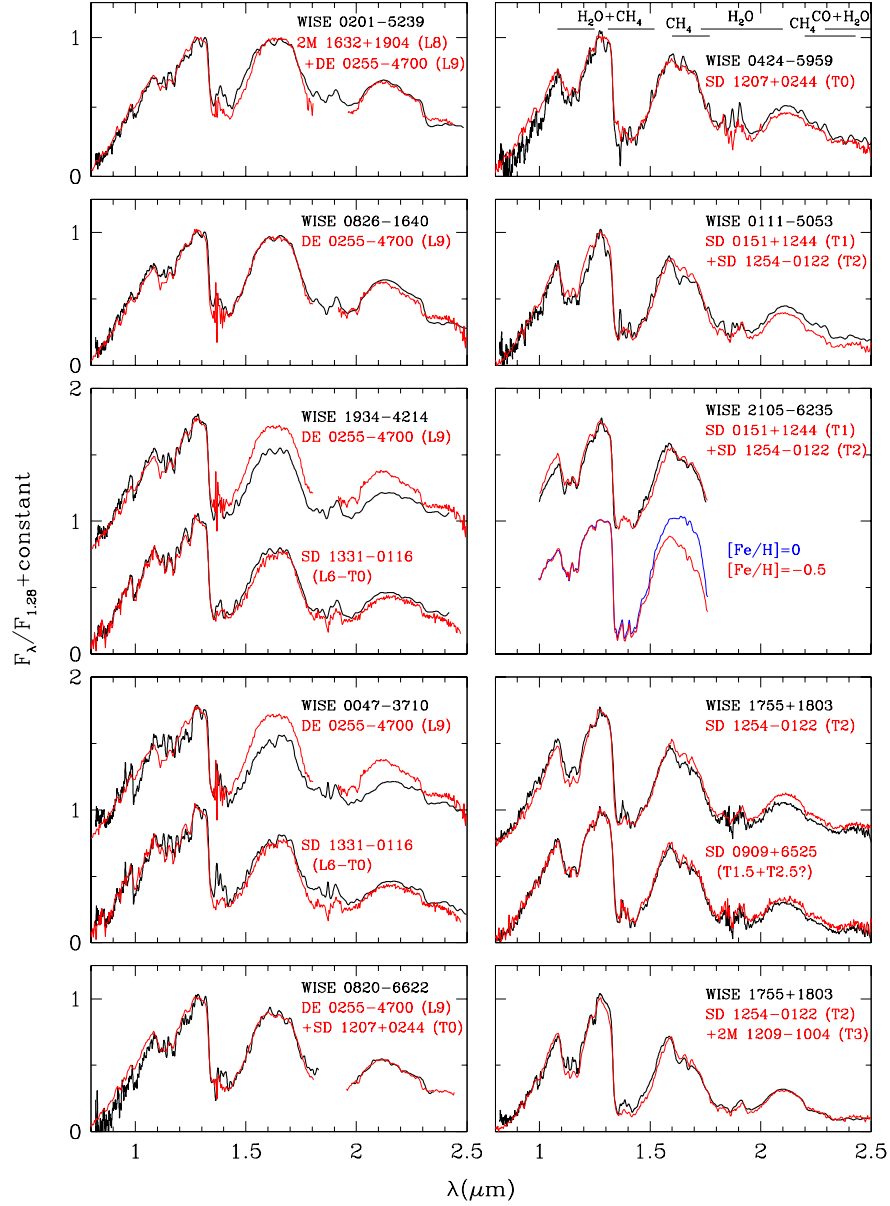


FIG. 7.— More near-IR spectra of high proper motion objects found with *WISE* (see Fig. 4). The panel for WISE 2105–6235 includes a comparison of model spectra from Burrows et al. (2006) for two values of $[\text{Fe}/\text{H}]$ at an effective temperature of 1400 K and a surface gravity of $\log g = 5$. The comparison spectra are from Burgasser et al. (2004, 2006, 2010), Burgasser (2007), Chiu et al. (2006), and Looper et al. (2007).